Control of mesoscale and nanoscale ordering of organic semiconductors at the gate dielectric/semiconductor interface for organic transistors†

Wi Hyoung Lee,[a] Jeong Ho Cho*[b] and Kilwon Cho*[a]

Received 20th November 2009, Accepted 12th January 2010
First published as an Advance Article on the web 12th February 2010
DOI: 10.1039/b924415h

In organic field-effect transistors (OFETs), the characteristics of the interface between the organic semiconductor and the gate dielectric are crucial determinants of device performance. We review recent progress in the control of mesoscale/nanoscale ordering of organic semiconductors at the gate dielectric. Issues concerning growth of the organic semiconductor on the surface-controlled gate dielectric, in-plane alignment of organic semiconductors, and self-assembled monolayers for organic semiconductors/dielectric are explored. We also discuss the effects of the molecular ordering and film morphologies of organic semiconductors on the electrical properties of OFETs.

1. Introduction

Organic field-effect transistors (OFETs) have received considerable attention because of their use in flexible, large area active display backplanes.[1–11] OFETs have a layered structure consisting of a gate electrode, gate dielectric, semiconducting layer, and source/drain electrodes (Fig. 1). Although all of the components and interfaces are important for correct functioning of OFETs, two types of interface govern the device performance of OFETs: the electrode/semiconductor interface for charge injection and the semiconductor/dielectric interface for charge transport. In bottom-gate OFETs as shown in Fig. 1, control of the semiconductor/dielectric interface can efficiently increase the field-effect mobility of OFETs because the surface characteristics of the dielectric can determine the growth of the semiconductor in the first few monolayers of the semiconductor near the semiconductor/dielectric interface.[12,13]

In order to control the dielectric surface properties for favorable mesoscale/nanoscale ordering of organic semiconductors, a common practice has been to insert an interfacial buffer layer such as a self-assembled monolayer (SAM) or a thin polymeric layer between the gate dielectric and the semiconductor because of the easy fabrication of such layers with nano-scale thickness. Furthermore, the presence of a buffer layer can reduce charge trapping states at the interface by covering silanol groups and ionic impurities of SiO_2.[14–17] The molecular ordering and film morphologies of organic semiconductors which are strongly affected by the π–π orbital overlap in conjugated molecules

[a]*Department of Chemical Engineering/Polymer Research Institute, Pohang University of Science and Technology, Pohang, 790-784, Korea. E-mail: kwcho@postech.ac.kr*
[b]*Department of Organic Materials and Fiber Engineering, Soongsil University, Seoul, 156-743, Korea. E-mail: jhcho94@ssu.ac.kr*
† This paper is part of a themed issue of *Journal of Materials Chemistry* on Interface engineering of organic and molecular electronics, guest edited by Alex Jen.

Jeong Ho Cho

Jeong Ho Cho is an assistant professor of Department of Organic Materials and Fiber Engineering at Soongsil University in Korea. He received his B.S. (2001) from Sogang University in Chemical Engineering, and M.S. (2003) and Ph.D. (2006) from POSTECH in Chemical Engineering. He was a postdoctoral researcher in Department of Chemical Engineering and Materials Science at University of Minnesota (2006–2008) and then joined the faculty at Soongsil University in 2008. His research interests include multifunctional fabrics, organic field-effect transistors, nonvolatile memory, and sensors.

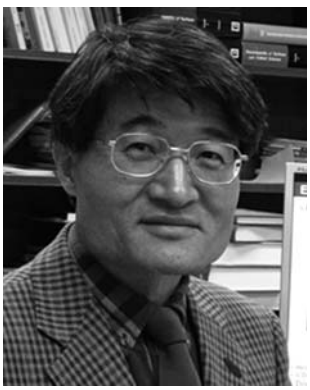

Kilwon Cho

Kilwon Cho is a full professor of Chemical Engineering and director of Polymer Research Institute at Pohang University of Science and Technology (POSTECH) in Korea. He received his B.S. (1980) and M.S. (1982) from Seoul National University (Korea) in applied chemistry and Ph.D. (1986) from the University of Akron in polymer science. He was a researcher at IBM Research Center (1987–1988) and then joined the faculty at POSTECH in 1988. His research interests include polymer surface, interface, thin-film and organic electronics. His current research interests are concerned with the development of printing-based organic field-effect transistors and organic photovoltaics.

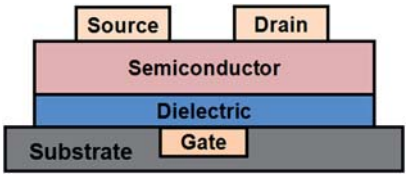

Fig. 1 Schematic representation of the bottom-gate/top-contact OFET structure.

determine the charge transport in the hopping process. For efficient charge transport from the source electrode to the drain electrodes, one-dimensional (1-D) anisotropic in-plane alignment of the semiconducting molecules is also desirable. Because a 1-D aligned film has a preferential anisotropic orientation of molecules, the 1-D structure exhibits higher field-effect mobility along the growth direction in device applications.

In this review, we discuss recent achievements in the control of the molecular ordering and film morphology of organic semiconductors near semiconductor/dielectric interfaces for high-performance OFETs. In Section 2, the growth of vacuum-deposited organic semiconductors is discussed, devoting particular attention to the use of surface treatment to induce desirable molecular orientations. In Section 3, we examine solution-processed organic semiconductors on a SAM-functionalized gate dielectric surface and one-dimensionally aligned solution-processed organic semiconductors. Furthermore, we discuss the use of SAMs as organic semiconductors and gate dielectrics. In Section 4, the future research perspective in OFETs is discussed.

2. Vacuum-processed organic semiconductors

Thin-film formation using the vacuum-deposition technique is a complicated process because many factors, including the deposition rate, substrate temperature, and substrate surface properties, affect the nucleation and growth of molecules.[18] The common growth modes can be categorized into three types: layer-by-layer, layer plus island, and island modes.[19] These growth modes are mainly determined by the interplay between molecule–molecule and molecule–substrate interactions.[20,21] Therefore, the substrate conditions such as roughness and chemical functionality critically affect the growth of the thin film, thereby governing the film morphology and molecular orientation of the organic semiconductor during vacuum deposition. Many research groups have reported the effects of substrate characteristics on the growth of pentacene, one of the most representative vacuum-deposited organic semiconductors (Fig. 2(a)). It is well known that pentacene molecules lie flat on highly interacting substrates such as clean Si and metal,[21–23] whereas they stand up on noninteracting substrates such as SiO_2 and SAM-treated SiO_2.[24,25] When pentacene molecules stand perpendicular to the substrate, charge carriers can be effectively transported along the parallel direction through the herringbone in-plane stacking. Although SAM-treated SiO_2 substrates usually induces this perpendicular orientation of pentacene molecules, a slight variation of the interaction between the pentacene and the SAM can change the grain morphology and microstructure of the pentacene molecules, resulting in dramatic differences in OFET performance.

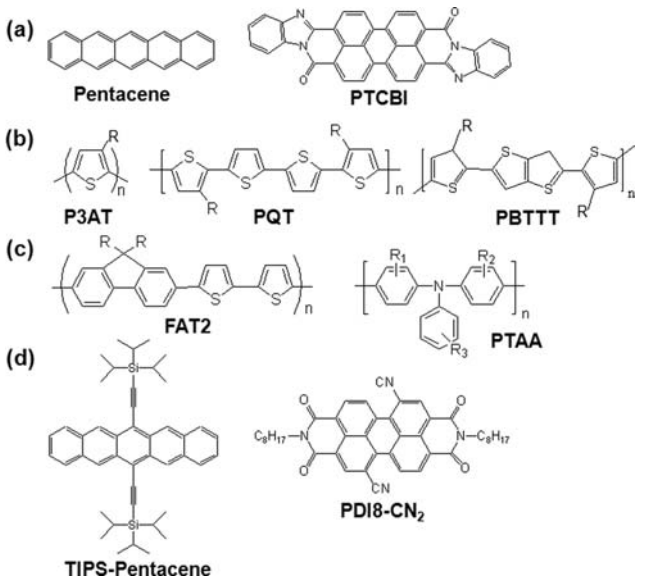

Fig. 2 Chemical structures of organic semiconductors discussed in this review. (a) Vacuum-processed organic semiconductors: pentacene and 3,4,9,10-perylenetetracarboxylic bis-benzimidazole (PTCBI). (b) Semi-crystalline polymeric semiconductors: poly(n-alkylthiophene) (P3AT), poly(n-alkylquarterthiophene) (PQT) and poly(2,5-bis(3-alkylthiophene-2-yl)thieno[3,2-b]thiophene) (PBTTT). (c) Amorphous polymeric semiconductors: poly(9,9-alkylfluorene-co-bithiophene) (FAT2) and polyarylamine (PTAA). (d) Solution-processed small-molecule semiconductors: bis-triisopropylsilylethynyl pentacene (TIPS-pentacene) and N,N′-bis(n-octyl)-(1,7&1,6)-dicyanoperylene-3,4:9,10-bis(dicarboximide) (PDI8-CN_2).

2.1. SAM-functionalized gate dielectric surface

SAMs are ordered molecular assemblies formed by the adsorption of active surfactants on a solid surface.[26] The order in these two-dimensional systems is produced by a spontaneous chemical reaction at the interface. This simple fabrication process makes SAMs easy to manufacture and thus technologically attractive for surface and interface engineering.[27] In OFET fabrication, to control the orientation and morphology of the organic semiconductor near the dielectric/semiconductor interface, many research groups have utilized SAM-treated metal oxides such as SiO_2 and Al_2O_3 as gate dielectrics.[28] SAM treatment of the metal oxide dielectric surface dramatically improves the performance of OFETs based on both solution- and vacuum-deposited organic semiconductors. The increased field-effect mobility afforded by SAM treatment has two origins: (1) improved molecular orientation and morphology of the first few semiconductor monolayers on the gate dielectrics, and (2) reduced density of the charge trapping state at the semiconductor–dielectric interface. Various types of SAMs, such as alkyl/aryl phosphonic acids, carboxylic acids, and organosilanes, can be applied to modify the metal oxide substrate in OFET fabrication.

2.1.1. Alkyl/aryl phosphonic and carboxylic acid-based SAMs. Alkyl/aryl phosphonic acid SAMs have been widely used to treat the metal oxide layer in OFETs due to their good stability to moisture and relative insensitivity to the density of hydroxyl groups on the metal oxide surface, as well as to the reduced

tendency of phosphonic acids to undergo homo-condensation.[29,30] Kelly and coworkers treated aluminium oxide with various alkyl/aryl phosphonic acid monolayers for high-performance OFETs, as shown in Fig. 3(a).[31] The field-effect mobility was 3.3 $cm^2 V^{-1} s^{-1}$ for the pentacene devices based on 1-phosphonohexadecane, which is a significant improvement compared with those based on untreated aluminium oxide. This mobility is close to that of single-crystal pentacene due to the formation of several molecular layers of near single-crystal-quality pentacene. The authors claimed that the chain length of the SAM molecules is a major factor in optimizing the performance of rough aluminium oxide surfaces. Jen and coworkers used aluminium oxide treated with anthrylalkylphosphonic acid SAMs as a gate dielectric.[32] They found that the introduction of this SAM improved the device performance in terms of the gate leakage current (*ca.* two orders of magnitude), on/off current ratio (one order of magnitude), and subthreshold slope down to 85 mV/decade; they attributed this improvement to a more favorable interface with the pentacene organic semiconductor arising from the similar chemical structures of anthracene and pentacene. Hill and coworkers inserted a phosphonate-linked anthracene SAM between silicon dioxide and pentacene (Fig. 3(b)).[33] Dramatic improvements in the subthreshold slope and threshold voltage were obtained compared with the devices without SAM treatment, the improvement being the result of a reduction in charge trapping states at the interface. The authors also reported the effect of alkyl chain length of n-alkyl phosphonic acid on pentacene growth and OFET performance, where the optimum performance was found to occur with a chain length of 8–10 carbon atoms.[34]

Alkyl carboxylic acids adsorb on metal oxides *via* an acid–base reaction. The driving force for alkyl carboxylic acid-based SAMs is the formation of a surface salt between the carboxylate anion and a surface metal cation. Because of their highly ordered and closely packed structure, similar to thiols on Au, alkyl carboxylic acid-based SAMs have been used on a wide range of metal oxide surfaces. In a study of pentacene film on aluminium oxide, Horowitz and coworkers found that the pentacene film structure could be drastically changed by modifying the surface with an eicosanoic acid SAM.[35,36] On bare Al_2O_3, the growth was initially two dimensional but changed to three dimensional with the formation of larger, though loosely connected grains. On the eicosanoic acid-treated SAM substrate, by contrast, the growth was three dimensional at all times (Fig. 3(c)).[36] In the SAM-treated device, the film is comprised of 3-D grains that present a better homogeneity in depth and a lower defect density, which results in a high field-effect mobility and stability. The gate voltage dependence of the field-effect mobility in these devices was investigated using both SAM-treated and untreated surfaces.

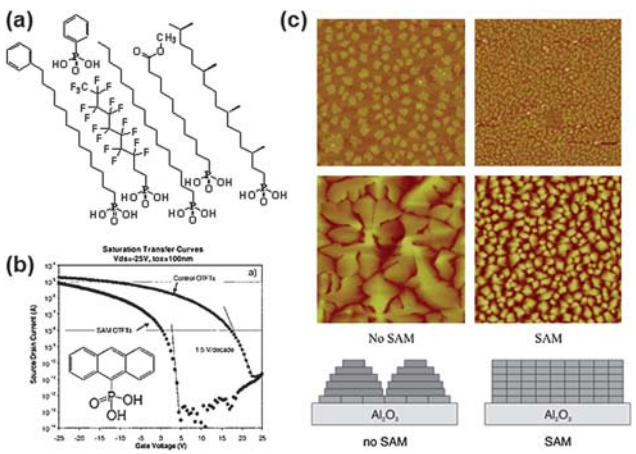

Fig. 3 (a) Molecular structures of phosphonic acid SAMs used for the surface treatment of the metal oxide surface. (Reproduced with permission from ref. 31, American Chemical Society.) (b) Transfer characteristics of OFETs with and without phosphonate-linked anthracene SAM. Inset shows the molecular structure of SAMs used in this study. (Reproduced with permission from ref. 33, American Institute of Physics.) (c) AFM images (4 μm × 4 μm) of pentacene films on bare (left) and SAM-modified (right) alumina with different coverage of 0.5 and 30 nm, and the schematic view of the pentacene structure grown on each surface. (Reproduced with permission from ref. 35 and 36, Elsevier.)

2.1.2. Organosilane-based SAMs. Organosilanes such as alkylchlorosilanes, alkylalkoxysilanes, and alkylaminosilanes are the most widely used materials as effective surface modifiers because of the uniform and reproducible surface properties they provide. For the surface reaction of organosilanes, hydroxylated substrates are required. For SiO_2 surfaces, the driving force for self assembly is the *in situ* formation of polysiloxane, which is connected to surface silanol groups (–SiOH) *via* Si–O–Si bonds. In 1997, Jackson and coworkers reported a dramatic improvement in OFET performance using octadecyltrichlorosilane (ODTS)-treated SiO_2 as a gate dielectric.[37] The devices exhibited field-effect mobilities as high as 1.5 $cm^2 V^{-1} s^{-1}$, on/off current ratios greater than 10^8, and near zero threshold voltages. Iwasa and coworkers reported that fluorinated SAMs on an SiO_2 gate dielectric can accumulate holes near the gate dielectric/semiconductor interface, resulting in a positive threshold voltage shift and increased field-effect mobility in pentacene transistors.[38]

Bao and coworkers investigated the pentacene crystalline structure deposited on an ODTS- or hexamethyldisilazane (HMDS)-treated SiO_2 substrate using conducting atomic force microscopy (C-AFM) and grazing-incidence X-ray diffraction (GIXD).[39] The faceted islands on HMDS showed a larger current flow than the dendritic islands on ODTS when C-AFM is applied on both surfaces. These single-crystal-like pentacene islands have fewer internal crystal defects and higher current flow than the dendritic islands (Fig. 4(a)). The morphology of ultra-thin layers correlates well with the field-effect mobility measured in OFETs. Li and coworkers treated an SiO_2 dielectric surface with phenyl-terminated silane molecules (PhTMS) to enhance the OFET performance. The treatment induced a change in the polymorphs' transformation from the triclinic bulk phase to the thin film phase and orthorhombic phase, which was strongly correlated with the OFET performance (Fig. 4(b)).[40] Park and coworkers systematically investigated the growth of pentacene crystals on monolayers of naphthol derivatives.[41]

Introduction of a SAM on the gate dielectric surface has also been found to enhance the crystal orientation and device performance of OFETs based on n-type semiconductors. Jabbour, DeLongchamp and coworkers reported that the unit cell orientation of n-type 3,4,9,10-perylenetetracarboxylic bis-benzimidazole (PTCBI) as shown in Fig. 2(a) changes with

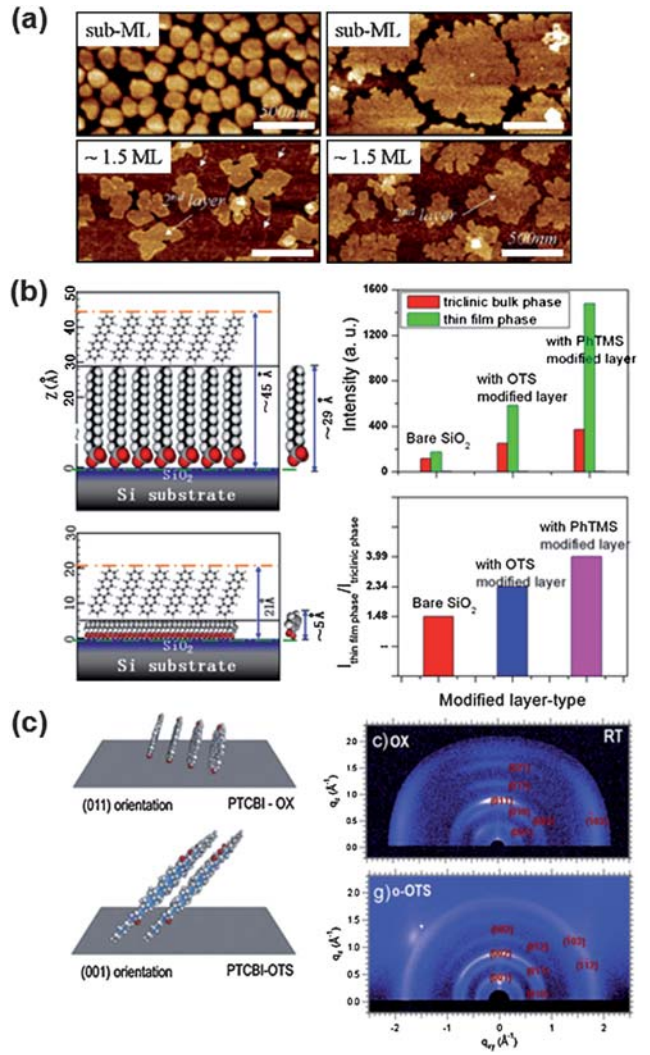

Fig. 4 (a) AFM images for submonolayer and ~1.5 ML films on HMDS- and ODTS-treated SiO_2/Si substrate, left and right, respectively. (Reproduced with permission from ref. 39, American Chemical Society.) (b) Schematic view of the interface between pentacene and ODTS- and PhTMS-treated SiO_2 gate insulator (left); diffraction peak intensities of thin film ($I_{thin\ film}$) and bulk phase (I_{bulk}) and ratio of diffraction peak intensities ($I_{thin\ film}/I_{bulk}$) of pentacene films on each surface. (right). (Reproduced with permission from ref. 40, Elsevier.) (c) PTCBI films with (011) and (001) orientations (left). 2-D GIXD images of 100 nm thick PTCBI films deposited on bare SiO_2 and ordered ODTS-treated SiO_2 surfaces (right). (Reproduced with permission from ref. 42, Wiley.)

dielectric surface treatment.[42] PTCBI films deposited on an oxide surface have an orientation of (011), while films on top of an ODTS-treated oxide surface have a preferred orientation of (001), as shown in Fig. 4(c). This preferred orientation enhances the lateral π-orbital overlap parallel to the source–drain plane, leading to high electron mobility values of 0.05 $cm^2\ V^{-1}\ s^{-1}$. Tokito and coworkers modified an SiO_2 surface with n-alkyltrichlorosilanes with various alkyl chain lengths (C_4–C_{18}) for high performance n-type OFETs based on thiazolothiazole derivatives.[43] The highest electron mobility of 1.2 $cm^2\ V^{-1}\ s^{-1}$ was achieved in devices with alkyl chains containing more than 14 carbons because of the suppression of the influence of electron trap sites on the SiO_2 gate insulator.

Dielectric surface functionalization using a hydrophobic CH_3-terminated SAM is well known to improve remarkably the crystalline nano- and microstructure, as well as the molecular orientation of the semiconductor. Typical ODTS and HMDS SAMs have been generally used to treat the metal oxide surface treatment in order to enhance device performance. However, for CH_3-terminated alkylsilane-treated SiO_2 surfaces, a wide range

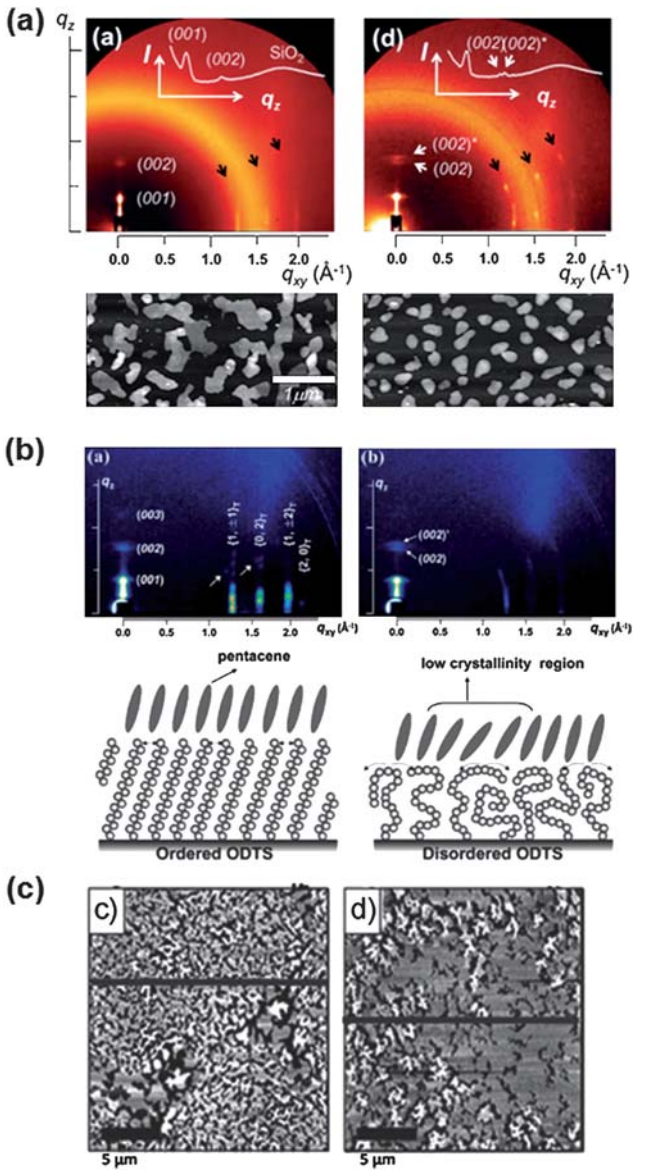

Fig. 5 (a) 2-D GIXD patterns and AFM images of nominal 2 ML-thick pentacene films deposited on the SiO_2 substrate treated with SAMs with different alkyl chain lengths of C8 (left) and C18 (right). (Reproduced with permission from ref. 44, Wiley.) (b) 2-D GIXD patterns of the 10 nm thick pentacene films and schematic diagrams of the pentacene structures deposited on the ordered and disordered ODTS monolayers. (Reproduced with permission from ref. 45, American Chemical Society.) (c) Nominally 3 nm thick pentacene films deposited onto ODTS with different densities (left: loose ODTS, right; dense ODTS). (Reproduced with permission from ref. 46, Wiley.)

of field-effect mobilities have been reported by many research groups, even though such surfaces have almost identical surface energies.[24,39,44–46] The research groups of Cho and Bao systematically studied these issues. Cho and coworkers demonstrated the variation in pentacene OFET performance depending on the alkyl chain length in the alkyl silane-treated SiO_2 substrate (Fig. 5(a)).[44] The pentacene films on organosilane SAMs with short alkyl chains showed laterally well-ordered crystal structures and large grains because of the higher diffusion mobility of pentacene molecules on the SAM-treated dielectric surface during the deposition, which causes the field-effect mobility to vary by more than a factor of 3 (up to values as high as 0.6 $cm^2\ V^{-1}\ s^{-1}$ for octyltrichlorosilane). Similarly, they investigated the effects of the phase state (order and disordered) of SAMs on the growth mode of pentacene films and OFET performance, as shown in Fig. 5(b).[45] Pentacene films grown on relatively highly ordered SAMs were found to have a higher crystallinity and a higher degree of interconnectivity between the pentacene domains, which directly serves to enhance the field-effect mobility, compared to films grown on disordered SAMs. The authors also observed the effect of substrate temperature on pentacene growth. Bao and coworkers deposited pentacene and C_{60} on ODTS monolayers with different 2-D phases prepared by Langmuir–Blodgett (LB) techniques.[46] They showed that an increase in the density of the methyl-terminated surface modification layer results primarily in two-dimensional growth of subsequently vacuum-deposited organic semiconductors (Fig. 5(c)). These changes in nucleation and growth give rise to a substantial improvement in the charge transport characteristics.

Cho and coworkers systematically studied the microstructural properties of a pentacene adlayer deposited on an ODTS SAM monolayer with varying the SAM grain size. Pentacene films deposited on an ODTS monolayer with a large SAM grain size exhibit better microstructural order of the pentacene molecules than do films deposited on a SAM with a small grain size because of the larger pentacene domain size and less heterogeneous crystalline structures in the former pentacene films.[47]

2.2. Polymeric layer-based gate dielectric surface

An attractive alternative approach to modifying metal oxide dielectric surfaces is to deposit a secondary polymeric layer. A key advantage of this approach is that spin-coated polymeric layer deposition is not limited by SAM–inorganic layer coupling, which determines the surface epitaxy and coverage of SAMs. Polymeric buffer layers have been generally inserted between the organic semiconductor and gate dielectrics to reduce the effect of surface roughness.[48] However, by varying the polymeric surface properties, such as the chemical functionality and hydrophobicity, the molecular orientation and morphology of the organic semiconductor film can be tuned over a wide range.

Yang and coworkers elucidated the crystalline morphologies and structures of thin pentacene films deposited on ultra-thin polymeric layer/SiO_2 bilayer gate dielectrics in which the surface hydrophobicity was controlled.[49] Polystyrene (PS), poly(4-vinylpyridine) (PVP), and poly(4-hydroxylstyrene) (PHS) were spin-coated onto the surface of an SiO_2 gate dielectric with a thickness of ~13 nm. Upon increasing the dielectric surface energy, the growth mode of pentacene crystals on these substrates changes from layer-by-layer to 3-D islands because of the different pentacene–substrate interactions. Chou and coworkers modified the SiO_2 surface with a photosensitive polyimide to match the surface free energy of the dielectric and that of the orthorhombic thin-film phase of the pentacene film.[50] The field-effect mobility of transistors was enhanced, reaching

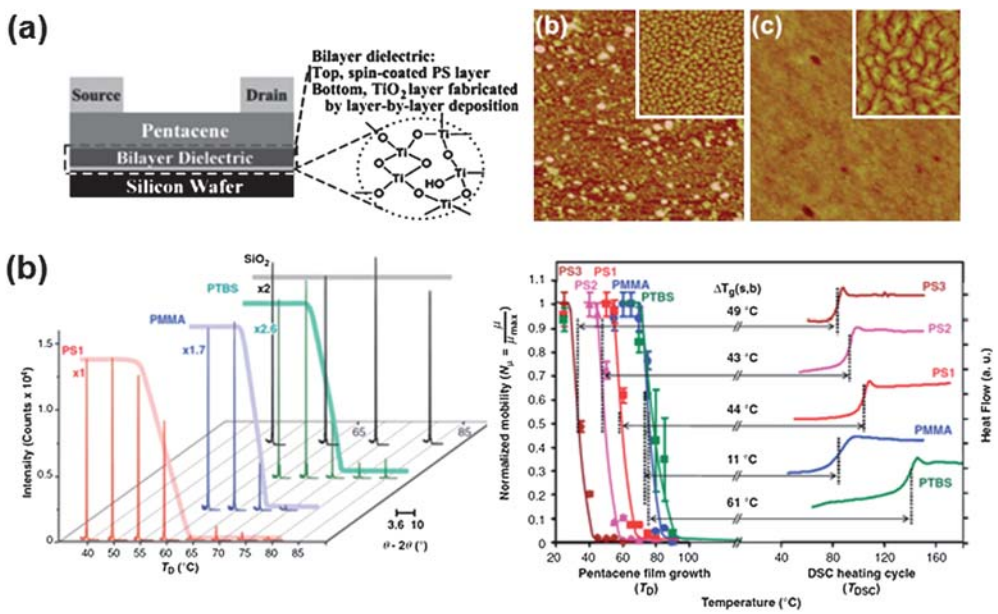

Fig. 6 (a) Schematic diagram of the structure of a top-contact OFET device with a TiO_2/PS bilayer dielectric (left) and AFM images of TiO_2 single dielectric (middle) and TiO_2/PS bilayer dielectric (right) and pentacene films deposited on each dielectric surface. (Reproduced with permission from ref. 51, American Institute of Physics.) (b) XRD data for 50 nm thick pentacene films (left) and carrier field-effect mobility (right) for pentacene OFETs fabricated at different deposition temperatures on various polymer/SiO_2 bilayer dielectrics. (Reproduced with permission from ref. 52, Science.)

values in excess of 2.0 $cm^2 V^{-1} s^{-1}$ due to the more complete first monolayer of pentacene on the gate dielectric surface. Cho and coworkers spin-coated PS onto layer-by-layer-deposited TiO_2.[51] The nonpolar PS top layer reduces the roughness of the dielectric, which results in low gate-leakage of the dielectric and a more ordered growth of the pentacene film, as shown in Fig. 6(a). Marks and coworkers reported a general approach to probe the effects of OFET semiconductor–dielectric interface chemistry on transistor performance using tailored polymer/SiO_2 bilayer dielectrics.[14] A nonpolar PS coating on SiO_2 with minimal gate leakage and surface roughness significantly enhances the field-effect mobilities of n-type and p-type transistors.

The influence of surface thermal behavior on overlying organic semiconductor film growth, film microstructure, and device performance should be addressed when choosing a polymeric layer. Marks and coworkers examined the effect of the viscoelastic properties of polymer gate-dielectric on the OFET performance.[52] They found that field-effect mobility drastically decreased at well-defined growth temperatures. The transition in carrier mobility was strongly correlated with dramatic microstructural and morphological changes of the semiconductor film at the surface glass transition temperature of the gate dielectric layer (Fig. 6(b)). They found that OFET performance measurements as a function of the semiconductor deposition temperature can be an informative probe for the polymer film viscoelastic properties. On the other hands, Hu and coworkers found that copper phthalocyanine (CuPc) molecules assemble under vacuum and on a solid surface through the combined effects of polymer chains reptation and the π–π interactions of CuPc.[53] Polycaprolactone (PCL) and poly(ethylene oxide) (PEO) were inserted between the CuPc semiconductor and the SiO_2 gate dielectric. At higher deposition temperatures, the intensified motion of the polymer chains causes the CuPc molecules to move and reorganize more easily. Films assembled by this method exhibited high electronic performance.

2.3. 1-D alignment of the gate dielectric surface

Charge carrier transport efficiency from source to drain electrodes is strongly dependent on the molecular chain ordering and crystalline orientation along parallel directions. 1-D alignment of the gate dielectric surface by mechanical rubbing or photoalignment was proposed for the orientation of organic semiconductors.[54] Malliaras and coworkers demonstrated that a rubbed poly(vinyl alcohol) (PVA) layer induces preferential orientation of pentacene grains along the rubbing direction, leading to enhanced pentacene mobility.[55] Tao and coworkers used a prerubbed SAM of n-alkyltrichlorosilane for the 1-D alignment of pentacene molecules along the source–drain channel direction.[56] Recently, Kim and coworkers systematically studied the orientation effect of pentacene films deposited on a rubbed polyimide layer under various conditions, such as the cumulative rubbing number and substrate temperature.[57]

3. Solution-processed organic semiconductors

Solution processing is a desirable film formation method for low-cost, large-area electronic devices. In particular, solution-processable polymeric semiconductors have received considerable attention because of their good solubility in common organic solvents, high field-effect electronic properties, and good film-forming properties.[58,59] Although some amorphous semiconductors with high field-effect mobilities have been reported in p-type and n-type organic semiconductors,[60–63] most polymeric semiconductors that show high field-effect mobilities are semicrystalline. Such semicrystalline polymeric semiconductors consist of conjugated backbones for effective π–π interactions between neighboring molecules and alkyl side chains for solubilizing these molecules (Fig. 2(b)). Considering two-dimensional charge transport parallel to the substrate in OFETs, lamellar stacking with edge-on alkyl side chain orientation, as shown in Fig. 7, is highly recommended.[64] Furthermore, interchain transport along the π–π stacking direction and intrachain transport along the main chain direction can facilitate efficient charge transport. On the other hand, disordered regions in a thin film can act as charge trapping sites, which significantly reduce the field-effect mobility. Thus, the formation of highly crystalline films with the above-mentioned molecular structure is a direct way to improve the field-effect mobility of OFETs based on polymeric semiconductors.

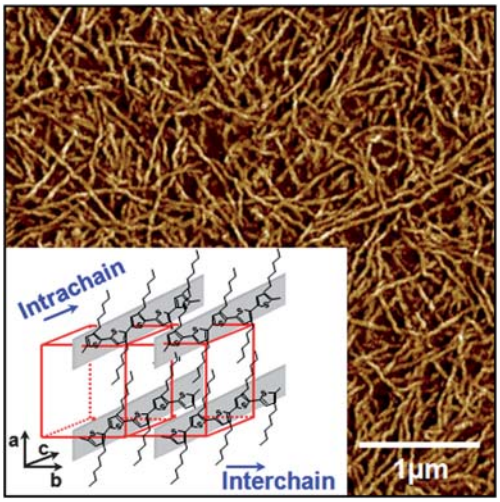

Fig. 7 AFM image of a P3HT thin film. Inset shows molecular packing structure of P3HT.

3.1. Surface-induced molecular ordering of polymeric semiconductors

Because dielectric surface characteristics determine the molecular ordering of semiconducting polymers during the solution-deposition or annealing process, fine tuning of the dielectric surface properties is required for high performance OFETs. As mentioned in Section 2, a SAM-treated metal oxide substrate directly serves as an ideal system for examining the effects of surface characteristics on the molecular orientation of polymeric semiconductors. Although SAM treatment of a metal oxide essentially induces molecular orientation along the surface normal direction, two-dimensional sheet-like lamellar stacking along the in-plane direction can be effectively facilitated through edge-on alkyl side chain orientation toward the surface normal (Fig. 7).[64] From this viewpoint, SAM treatment can improve the

electrical properties of OFETs based on polymeric semiconductors by promoting such a molecular orientation. In this section, we mainly focus on the molecular orientations and film morphologies of organic semiconductors; surface dipole and charge trapping are not explicitly discussed, notwithstanding their importance in OFET characteristics. In solution-processed OFETs, organosilanes have been generally used to treat gate dielectric surfaces; hence, only surface treatment using organosilane-based SAMs will be considered in this section.

Sirringhaus and coworkers reported that spin-cast regioregular poly(3-hexylthiophene) (P3HT) films on an HMDS-treated silicon substrate yielded high field-effect mobilities in excess of 0.1 $cm^2\ V^{-1}\ s^{-1}$.[58,65,66] They explained their findings by the hypothesis that HMDS treatment removes residual water and polar groups on SiO_2, leading to an increase in field-effect mobility. Veres and coworkers found that dielectric surface treatment significantly affects the field-effect mobility of OFETs based on P3HT, polyarylamine (PTAA), and poly(9,9-dioctylfluorene-co-bithiophene) (F8T2) (see Fig. 2(c) for chemical structure).[67] Specifically, they found that the field-effect mobility increased with increasing surface hydrophobicity. From the improvement in field-effect mobility of OFETs based on *amorphous* PTAA by ODTS treatment, the authors claimed that dielectric surface treatment may neutralize surface defects, while inducing molecular orientation of the organic semiconductor. Brutting and coworkers also found that treatment of an SiO_2 dielectric surface with a hydrophobic ODTS SAM enhanced the performance of a P3HT FET.[68] They attributed the increase in field-effect mobility to changes in the structural organization of P3HT near the dielectric interface; however, they did not perform experiments to test this hypothesis.

McGehee and coworkers demonstrated that HMDS or ODTS treatment of an SiO_2 dielectric surface strongly affects the molecular orientation of P3HT at the insulator–semiconductor interface.[69,70] To study the orientation of crystals in a direction substantially parallel to the substrate, the mosaic distribution of edge-on crystallites was investigated by measuring the rocking curves at (100) for P3HT films onto substrates with different surface characteristics (Fig. 8(a)). Note that the (100) reflection in XRD represents edge-on molecular orientation in P3HT as shown in Fig. 7. P3HT films on an ODTS-treated substrate had well-oriented edge-on crystallites compared with those on an HMDS-treated substrate. The rocking curves of P3HT films with different film thicknesses on the ODTS-treated surface imply that highly oriented crystals nucleated at the film–substrate interface. Upon increasing the P3HT film thickness, the amount of marginally oriented crystals gradually increased because well-oriented crystals are buried at the interface near the ODTS

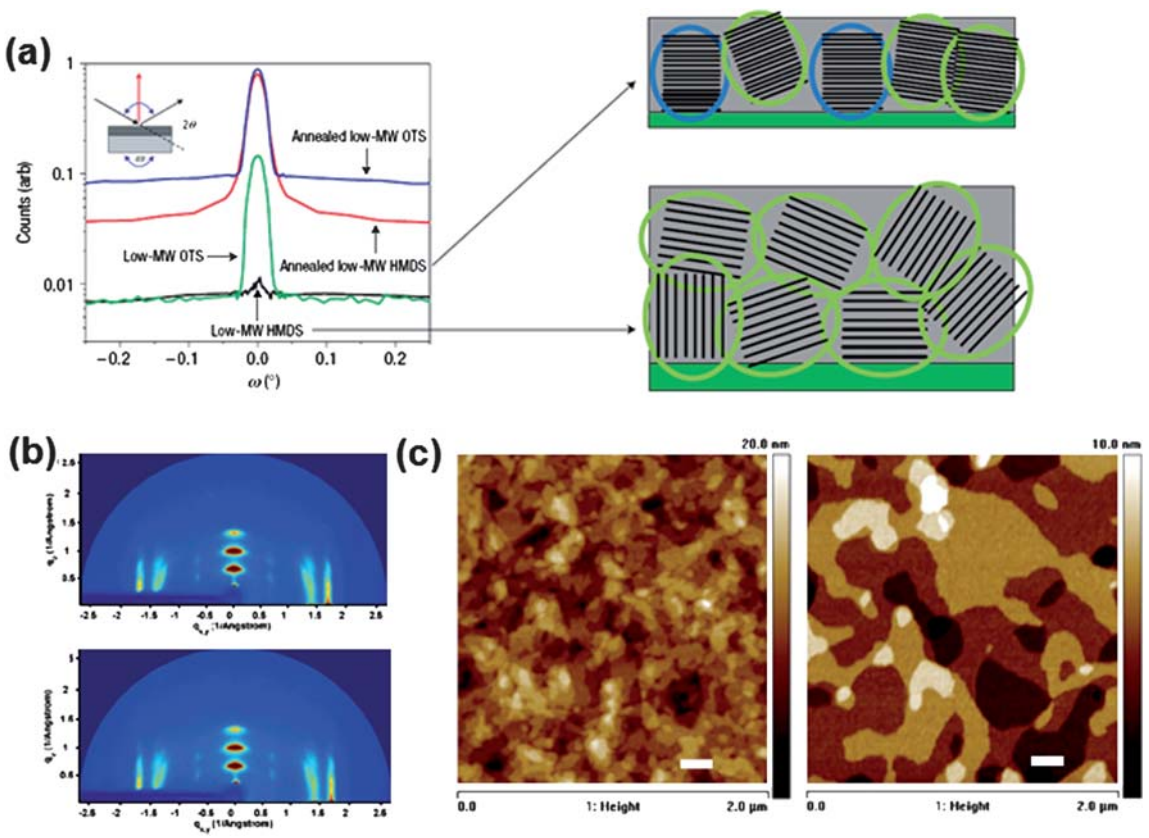

Fig. 8 (a) Rocking curves performed on the (100) peaks for the P3HT films on ODTS/HMDS-treated substrate and schematic P3HT molecular orientation. The left inset shows the rocking-curve geometry and the corresponding angles relative to the sample normal ω. (Reproduced with permission from ref. 70, Nature Publishing Group.) (b) 2-D GIXD of PBTTT films on different substrates. Top: on bare SiO_2 after 180 °C annealing, bottom: on OTS/SiO_2 after 180 °C annealing. (Reproduced with permission from ref. 82, American Chemical Society.) (c) AFM image of PBTTT film on bare SiO_2 (left) and OTS/SiO_2 (right) after 180 °C annealing. (Reproduced with permission from ref. 83, American Institute of Physics.)

surface, whereas poorly oriented crystals originate from the bulk film. Although many research groups have examined the effects of gate dielectric surface treatment on the molecular structure of organic semiconductors and the electrical properties of OFETs, the mechanisms determining the different orientations of the organic semiconductors molecules are not fully understood.

Cho and coworkers studied the effect of the interaction between SAMs and P3HT molecules on the structural changes of the melt-crystallized P3HT film.[71–73] Depending on the end-functionality of the SAMs, P3HT adopts different molecular orientations, as confirmed by XRD, near-edge X-ray absorption fine structure (NEXAFS) spectroscopy, and AFM. The high field-effect mobilities of P3HT FETs based on amine-functionalized SAMs were explained by the preferential P3HT edge-on orientation induced by the repulsive interaction between the thienyl backbone in P3HT molecules and the unshared electron pairs in amine-functionalized SAMs.

In the case of poly(n-alkyl thiophene), the lamellar stacking between molecules is increased by the interaction between the noninterdigitated side chains as the alkyl side chain length increases.[74] However, the field-effect mobility of poly(n-alkyl thiophene)s with a long side chain was found to be low, mainly because of the increase in the insulating portion in the molecules.[75,76] Liquid crystalline poly(3,3‴-didodecylquaterthiophene) (PQT-12) with long alkyl side chains was reported to show a high field-effect mobility (>0.1 $cm^2 V^{-1} s^{-1}$) because of the well-resolved lamellar ordering with π–π stacking along the parallel direction induced by the interdigitated alkyl side chains.[74,77,78] Similar to the case of P3HT OFETs, surface treatment has been found to increase the field-effect mobility of OFETs based on PQT-12 film.[78] Ong and coworkers found that octyltrichlorosilane (OTS) was optimum for achieving high field-effect mobilities in OFETs based on PQT-12 film.[79] However, a detailed structural analysis of PQT-12 films has not been performed. In addition, the authors developed a versatile approach to dielectric surface modification using self-crosslinked poly(methyl silsesquioxane).[80] The high concentration of methyl groups in poly(methyl silsesquioxane) increases the molecular ordering of PQT-12, yielding field-effect mobilities up to 0.15 $cm^2 V^{-1} s^{-1}$.

Poly(2,5-bis(3-alkylthiophene-2-yl)thieno[3,2-b]thiophene) (PBTTT) with fused thiophene was reported to exhibit well-ordered liquid crystalline characteristics and high field-effect mobility in OFET applications.[81] In agreement with the results for PQT-12, OFETs based on PBTTT film on an OTS-treated SiO_2 substrate showed high field-effect mobilities. Chabinyc and coworkers studied the correlation between the thin-film structure of PBTTT and its electrical properties in OFET devices using 2-D GIXD, as shown in Fig. 8(b).[82] Thermal annealing of PBTTT film at the mesophase increases the edge-on molecular orientation of PBTTT molecules, regardless of whether the gate dielectric is untreated SiO_2 or OTS-treated SiO_2. From an AFM analysis of the mesoscale morphology, as shown in Fig. 8(c), the PBTTT film on an OTS-treated substrate was found to consist of large crystallites (grain size ~ 200 nm), whereas the film on bare SiO_2 was comprised of small crystallites because of the increased nucleation density. The high surface mobility of PBTTT polymer on the hydrophobic OTS substrate may induce favorable interactions between PBTTT molecules, resulting in a large grain size of PBTTT and a high field-effect mobility. DeLongchamp and coworkers also studied the effect of OTS treatment on PBTTT microstructure using NEXAFS spectroscopy.[83] After thermal annealing of the PBTTT films, the dichroic ratio of PBTTT molecules increased on the OTS-treated SiO_2 substrate, whereas the ratio remained unchanged on the bare SiO_2 substrate. The low measured dichroic ratio on bare SiO_2 is directly correlated with the higher portion of misorientation in the disordered region, as confirmed by a greater number of grain boundaries in the AFM image (Fig. 8(c)).

Tokito and coworkers studied the effect of ODTS surface treatment time on the electrical performance of PBTTT OFETs.[84] Upon increasing the ODTS treatment time, the surface became hydrophobic and smooth, which induced the further edge-on orientation of PBTTT molecules. The optimal π–π stacking along the in-plane direction induced by the increased edge-on orientation led to an increase in the field-effect mobility. The authors additionally changed the dielectric surface characteristics by using SAMs with different functional groups.[85] Fluorinated SAM-based PBTTT OFETs showed the best electrical performance, which is attributed to better edge-on orientation of PBTTT induced by the reduced interaction of PBTTT with hydrophobic fluorinated SAMs.

Surface-induced molecular ordering of representative polymeric semiconductors (P3HT, PQT-12, and PBTTT) has been examined, focusing in particular on dielectric surface treatment using SAMs. Because many other molecular and processing factors—including regioregularity,[64] molecular weight,[86,87] side chain length,[75,76] solvent power,[66] film-forming method,[88] and post-treatment annealing[77,82]—also affect the molecular orientation and film morphology of organic semiconductors, optimizing the dielectric surface properties with other molecular and processing parameters is highly desirable for further improvement in field-effect electronic characteristics.

3.2. Alignment of solution-processed semiconductors

For efficient charge transport along the in-plane direction in OFETs, one-dimensional (1-D) anisotropic in-plane alignment of the semiconducting molecules is desirable. Many fabrication methods including rubbing,[89,90] friction-transfer techniques,[91] photoalignment,[92] and LB deposition[93] have been utilized to align the molecules laterally. Comprehensive review articles on the controlled deposition of organic semiconductors involving a patterning process are available.[94,95] Here, we focus on the structures of organic semiconductors induced by an in-plane molecular alignment method. Alignment of polymeric semiconductors and solution-processed small-molecule semiconductors are discussed.

3.2.1. In-plane alignment of polymeric semiconductors. Preferential backbone alignment by applying a shear force on the polymer chain was reported by Nagamatsu and coworkers.[96,97] They demonstrated P3HT chain alignment by the friction transfer technique (Fig. 9(a) left), which is well known for fabricating thin films with strong in-plane anisotropy. The P3HT backbone is aligned along the drawing direction, resulting in high field-effect mobility in devices with the channel parallel to the alignment direction. In a related approach, Damman and

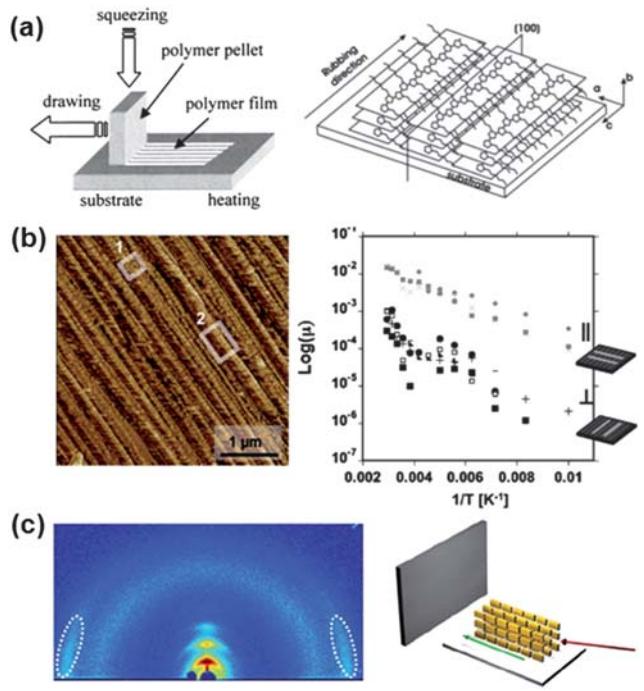

Fig. 9 (a) Schematic diagram of the friction-transfer process (left). (Reproduced with permission from ref. 97, American Institute of Physics.) Schematic structure of the aligned P3HT film after the friction-transfer process or nanorubbing process (right). (Reproduced with permission from ref. 98, American Chemical Society.) (b) AFM phase image of a directionally crystallized P3HT thin film using TCB for epitaxy (left). The box labeled 1 outlines a region with equiaxial crystallites. The box labeled 2 outlines a region with elongated crystallites. Temperature-dependent mobility measurements for a number of different devices, with parallel (gray symbols) and perpendicular (black symbols) orientations (right). The different symbols represent different devices. (Reproduced with permission from ref. 102, Wiley.) (c) 2-D GIXD of dip-coated higher-molecular-weight CDT-BTZ films after annealing. The patterns were recorded parallel to the dipping direction (white dashed lines point toward the scattering from the in-plane π-stacking). The green arrow in the schematic drawing indicates the dipping and alignment direction, while red corresponds to the incident X-ray beam. (Reproduced with permission from ref. 103, Wiley.)

coworkers employed a nanorubbing method using an AFM tip to fabricate highly oriented P3HT films.[98] Their work successfully demonstrated that a nanoscale shear force can orient the P3HT backbone along the rubbing direction (Fig. 9(a) right).

Anisotropically aligned polymeric semiconductors formed by using a predeposited alignment layer have been reported by several research groups. Sirringhaus and coworkers demonstrated that liquid-crystalline F8T2 polymer can be aligned along the backbone direction by placing the polymer in contact with a mechanically rubbed polyimide alignment layer.[99] OFETs based on aligned F8T2 film showed higher field-effect mobility with the channel parallel to the alignment direction than with the channel perpendicular to the alignment direction. Brinkmann and coworkers used 1,3,5-trichlorobenzene (TCB) to induce directional crystallization of P3HT. They found that TCB can induce epitaxial growth of P3HT where the backbone orientation is parallel to the long axis of the TCB crystal.[100,101] Salleo and coworkers applied this method to OFETs and examined the anisotropy of charge transport in directionally crystallized P3HT thin films (Fig. 9(b)).[102] They found that charge transport along the fiber growth direction, which corresponds to the backbone direction, is more facilitated compared to that along the fiber normal direction. This observation was illustrated by the existence of fiber-to-fiber grain boundaries, as shown in the AFM image (Fig. 9(b)), which reduces electrical connectivity in the fiber normal direction.

Although the use of a predeposited alignment layer or friction transfer *via* a solid pallet produced well-oriented polymeric layers with preferential backbone alignment, the formation of aligned polymer semiconductor layers directly from the solution process is highly desirable. Groves and coworkers used the LB method to fabricate anisotropic P3HT films with high field-effect mobilities of up to 0.02 $cm^2\ V^{-1}\ s^{-1}$. In their work, the alignment of the backbone was induced at the meniscus of the liquid–air interface during the LB deposition process.[93] Mullen and coworkers reported that cyclopentadithiophene-benzothiazole copolymer (CDT-BTZ) can be aligned using the dip-coating method.[103] OFETs based on CDT-BTZ film showed high field-effect mobilities up to 1.4 $cm^2\ V^{-1}\ s^{-1}$, where the improvement in mobility is directly correlated with the enhanced intrachain charge transport arising from the alignment of the CDT-BTZ backbone during the dip-coating process (Fig. 9(c)). DeLongchamp and coworkers demonstrated that terraced PBTTT ribbons can be easily fabricated using a flow coating process and subsequent annealing at the backbone melting temperature.[104] These ribbons exhibited a unique in-plane structure with backbone alignment along the flow direction, where the π–π stacking is perpendicular to the flow direction. Notwithstanding the difference in the introduced coating methods and materials, the polymer backbone is preferentially aligned along the direction of the shear force.

3.2.2. Alignment of solution-processed small-molecule semiconductors. Solution-processed small-molecule semiconductors have attracted much attention because of their printability and high field-effect mobilities in OFET applications.[105,106] A recent review article by Cho and coworkers focused on the morphological and structural evolution of small-molecule semiconductors during the solution-deposition process.[107] Here, the main focus is the "*one dimensional*" alignment for efficient charge transport from the source to the drain electrodes. Mullen and coworkers developed a zone-casting technique to deposit substituted hexaperibenzocoronene (HBC) (Fig. 10(a)).[108] By changing the solution supply and velocity of the moving support, the solution evaporation rate was controlled such that uniaxially aligned HBC columns with intercolumnal π–π stacking were formed. In a related approach, Sirringhaus and coworkers produced directionally assembled pentacene by zone-casting.[109] The pentacene film showed a packing structure close to that of "bulk-phase" pentacene, with preferential in-plane alignment (*a*-axis of the unit cell) along the zone-casting direction.

Controlling molecular assembly in a solution by inducing flow in the solution is also a desirable approach to fabricating 1-D aligned structures. Cavallini and coworkers fabricated the 1-D aligned alternate block-oligomer, terthiophene-bis-fluorene, by using microinject molding in capillaries, as shown in

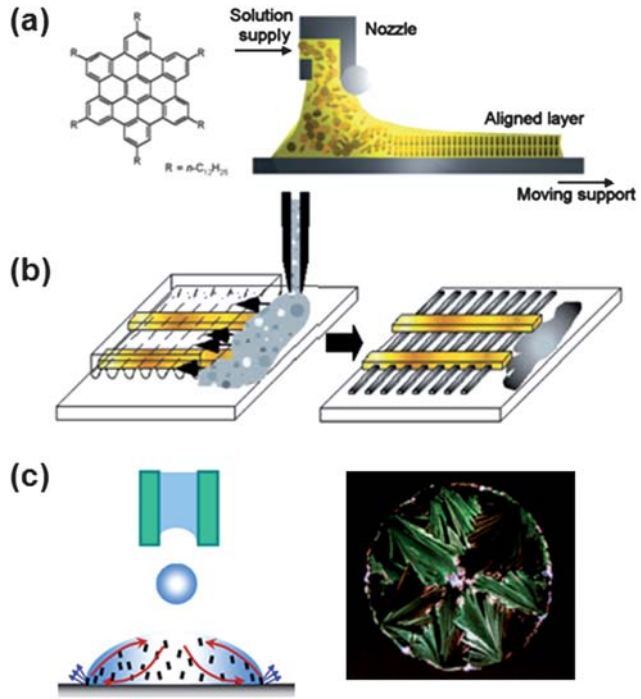

Fig. 10 (a) Chemical structure of discotic HBC derivatives and a schematic of the zone-casting technique. (Reproduced with permission from ref. 108, Wiley.) (b) Schematic representation of the deposition process, showing the steps related to micromolding in capillaries and lithographically controlled wetting. (Reproduced with permission from ref. 110, American Chemical Society.) (c) Schematic representation of the inkjet printing process with evaporation-induced flow in a droplet (left). Polarized optical microscopy image of ink-jet printed TIPS-pentacene droplets with chlorobenzene/dodecane (80/20) mixed solvent (right). (Reproduced with permission from ref. 114, Wiley.)

Fig. 10(b).[110,111] The fabricated nanostrips in capillaries were aligned with an intermolecular distance of approximately 4 Å, which led to a high field-effect mobility along the nanostrip direction. Cho and coworkers demonstrated that drop-casting bis-triisopropylsilylethynyl pentacene (TIPS-pentacene) solution onto a inclined substrate is a direct way to fabricated 1-D microcrystal arrays (see Fig. 2(d) for chemical structure).[112] Uniaxially aligned TIPS-pentacene crystal arrays showed a high field-effect mobility of 0.3 $cm^2\ V^{-1}\ s^{-1}$ in OFET applications, which directly correlated with the preferential orientation of TIPS-pentacene crystals along the *a*-axis. Salleo and coworkers used this method for fabricating the aligned N,N′-bis(n-octyl)-(1,7&1,6)-dicyanoperylene-3,4:9,10-bis(dicarboximide) (PDI8-CN_2) film with strong charge transport anisotropy.[113] They found that 1-D growth of the PDI8-CN_2 crystals was attributed to the drying behavior at the inclined substrate. Cho and coworkers also studied the evaporation behavior of ink-jet printed TIPS-pentacene droplets (Fig. 10(c)).[114] Self-aligned crystals from the edge to the center of the droplet were fabricated using a mixed solvent through control of the evaporation-induced flow in a droplet. Furthermore, the effect of surface energy on the morphological and structural development in ink-jet printed TIPS-pentacene droplets was investigated.[115] By visualizing the drying droplet, the authors confirmed that the formation of self-aligned crystals on a hydrophilic surface is due to contact line pinning and outward convective flow in the drying droplet.

3.3. Self-assembled monolayers as organic semiconductors and gate dielectrics

Self assembly is an emerging technology for bottom-up fabrication of nanostructures. A π-conjugated molecule can be deposited as a monolayer by means of self assembly. Using the LB method, OFETs based on a monolayer semiconductor have been fabricated and shown to exhibit excellent performance.[93,116] However, the prepared semiconducting monolayers were easily delaminated because there were no binding sites between the gate dielectric and LB-deposited semiconductor.

Recently, π-conjugated molecules capable of binding to the gate dielectric surface were reported by some research groups, and used as the basis for self-assembled monolayer field-effect transistors (SAMFETs). Because in-plane π–π stacking is rather limited by the bonding to the substrate, a new class of molecules with adequate binding to the substrate as well as π–π in-plane stacking should be developed to achieve high performance SAMFETs. Nuckolls and coworkers studied SAMFETs based on a tetracene molecule with a terminal catechol that chelates strongly with metal oxides, thereby forming a uniform monolayer, as shown in Fig. 11(a).[117] Although the molecular packing structure was not fully examined, gate-field modulation was observed at low source–drain voltage. In an extension of this work, they used a hexabenzocoronene with a carbonyl moiety that could bind to the SiO_2 substrate.[118] The chemoresponsive performance of field-effect transistors in which a monolayer was used as the active layer between nanogap electrodes was also examined. Horowitz and coworkers fabricated SAMFETs using bifunctional molecules with a short alkyl chain linked to the oligothiophene moiety.[119] A well-organized monolayer with an RMS roughness of 0.2 nm was formed on the Al_2O_3 substrate after dipping in the solution for tens of minutes. Field-effect mobilities of approximately $10^{-3}\ cm^2\ V^{-1}\ s^{-1}$ at a channel length below submicron size were obtained. De Leeuw and coworkers developed SAMFETs with strong π–π intermolecular coupling (Fig. 11(b)) using a molecule that consists of α-substituted quinquethiophene as the semiconducting part and undecane as the spacer for promoting anisotropic ordering.[120,121] Herringbone-type in-plane stacking was suggested from the Bragg rod diffraction patterns of these SAMs. Field-effect mobilities above $0.01\ cm^2\ V^{-1}\ s^{-1}$ were obtained with high reproducibility.

In a parallel approach, SAMs with a thickness of approximately 2–3 nm have been shown to be viable alternatives to common thick dielectrics such as SiO_2 and Al_2O_3. Vuillaume and coworkers used COOH-terminated SAMs as a dielectric in oligothiophene OFETs.[122] Halik, Klauk and coworkers demonstrated that pentacene FETs can be fabricated using 18-phenoxyl-octadecyltrichlorosilane as the SAM dielectric (Fig. 11(c)).[123] In an extended work, they used two types of SAMs, n-octadecyl-phosphonic acid or n-octadecyltrichlorosilane, as the gate dielectric.[124] Organic complementary circuit was fabricated using more densely packed phosphonic acid SAMs with lower gate leakage current. Cho and coworkers also demonstrated P3HT-based OFETs with docosyltrichlorosilane SAM as gate

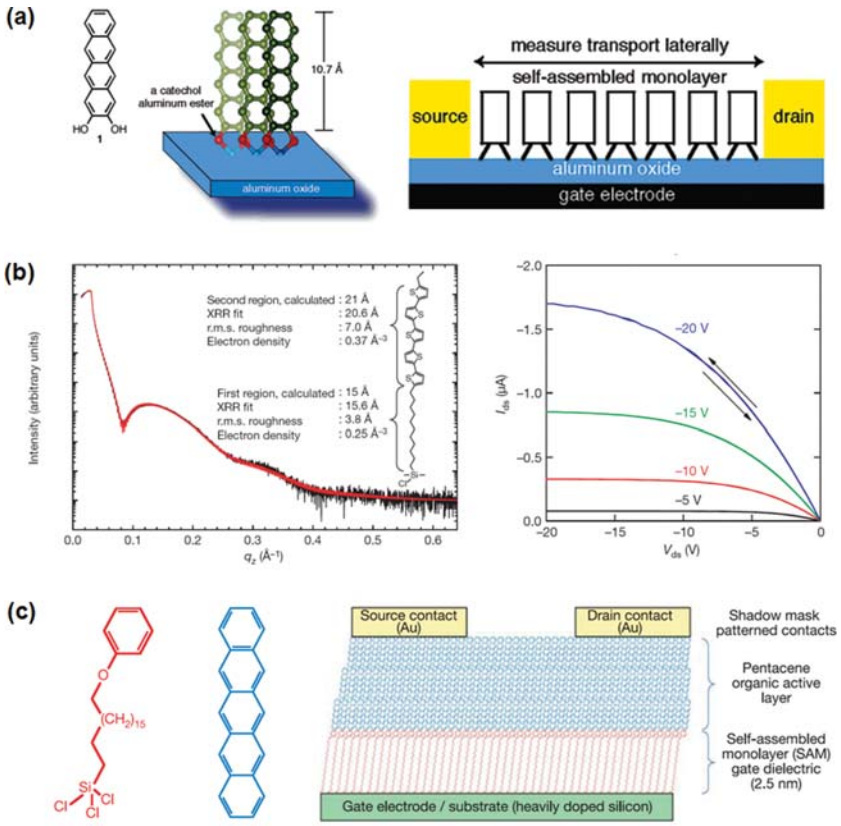

Fig. 11 (a) Schematic bonding and orientation of end-functionalized tetracene (left). Schematic of a self-assembled monolayer transistor (right). (Reproduced with permission from ref. 117, American Chemical Society.) (b) X-Ray reflectivity of a SAM on silicon dioxide. The inset shows the chemical structure of the molecule and the thickness, RMS roughness values and electron densities obtained from the fit (left). Output characteristics for the corresponding SAMFET (right). (Reproduced with permission from ref. 120, Nature Publishing Group.) (c) Chemical structure of 18-phenoxy-octadecyltrichlorosilane and pentacene (left). Cross section of a pentacene FET with a molecular SAM dielectric (right). (Reproduced with permission from ref. 123, Nature Publishing Group.)

dielectric.[125] SAM-based FETs open a new approach to the bottom-up fabrication of organic transistors because of their simple fabrication process and molecular-scale thickness.

4. Future research perspective

Surface treatment of inorganic gate-dielectrics such as SiO_2 and Al_2O_3 has been intensively studied for high performance OFETs. However, for the realization of low-cost/flexible OFETs, the control of the molecular orientation and film morphologies of organic semiconductors on polymeric gate-dielectrics will be technically important issues. In addition, the structural organization of organic semiconductors during the formation of the film using high throughput printing-based deposition techniques such as inkjet printing and gravure printing is an interesting area for the low-cost, large-area fabrication of OFETs. Furthermore, the OFET performance based on n-type organic semiconductors should be enhanced by applying various processing methods used in p-type semiconductor based devices for controlling the molecular ordering.

The control of molecular ordering of organic semiconductors at the gate-dielectric/semiconductor interface is important not only for enhancing field-effect mobility but also improving device stability under bias stress.[126] Because the bias stability strongly depends on the charge trapping sites induced by the structural defects of the organic semiconductor films, a systematic study on the change of the structural defects by controlling the molecular ordering of organic semiconductors should be needed. The correlation between the molecular ordering and device stability will be the major concerns for the application of OFETs in display backplanes.

5. Conclusions

We have reviewed recent achievements in the control of meso-scale/nanoscale ordering of organic semiconductors at the gate dielectric. The addition of SAMs and thin polymeric layers onto the dielectric significantly affected the growth of organic semiconductors by changing the interaction between organic semiconductors and SAMs, which resulted in a dramatic difference in molecular ordering and film morphologies of the organic semiconductor layer and its field-effect mobility in device applications. Furthermore, in-plane alignment of organic semiconductors was induced using a gate dielectric alignment layer, applying a shear force, or controlling the drying process. These methods led to 1-D growth of the organic semiconductor on the gate dielectric surface during the vacuum- or solution-deposition process. OFET performances of 1-D aligned organic

semiconductors were superior when the alignment direction was parallel to the source–drain channel direction. Because not only the structure of the organic semiconductors near the gate dielectric but also other parameters such as surface defects, polarity, and roughness of the dielectric can affect charge transport near semiconductor/gate dielectric interfaces, a comprehensive understanding of the charge transport mechanism is needed in order to optimize the electrical properties of OFETs.

Acknowledgements

This work was supported by a grant (F0004021-2009-32) from the Information Display R&D Center under the 21st Century Frontier R&D Program, and the National Research Foundation of Korea (NRF) grant (2010-0000757). The authors thank the Pohang Accelerator Laboratory for providing the synchrotron radiation sources at 3C2, 4C1, 4C2, 8C1, and 10C1 beam lines used in this study.

References

1 G. Horowitz, *Adv. Mater.*, 1998, **10**, 365.
2 C. J. Drury, C. M. J. Mutsaers, C. M. Hart, M. Matters and D. M. de Leeuw, *Appl. Phys. Lett.*, 1998, **73**, 108.
3 Y. L. Loo and I. McCulloch, *MRS Bull*, 2008, **33**, 653.
4 A. Facchetti, *Mater. Today*, 2007, **10**, 28.
5 S. Allard, M. Forster, B. Souharce, H. Thiem and U. Scherf, *Angew. Chem., Int. Ed.*, 2008, **47**, 4070.
6 D. Braga and G. Horowitz, *Adv. Mater.*, 2009, **21**, 1473.
7 D. J. Gundlach, J. E. Royer, S. K. Park, S. Subramanian, O. D. Jurchescu, B. H. Hamadani, A. J. Moad, R. J. Kline, L. C. Teague, O. Kirillov, C. A. Richter, J. G. Kushmerick, L. J. Richter, S. R. Parkin, T. N. Jackson and J. E. Anthony, *Nat. Mater.*, 2008, **7**, 216.
8 J. H. Cho, J. Lee, Y. Xia, B. Kim, Y. Y. He, M. J. Renn, T. P. Lodge and C. D. Frisbie, *Nat. Mater.*, 2008, **7**, 900.
9 Y. D. Park, H. S. Lee, Y. J. Choi, D. Kwak, J. H. Cho, S. Lee and K. Cho, *Adv. Funct. Mater.*, 2009, **19**, 1200.
10 L. Z. Qiu, W. H. Lee, X. H. Wang, J. S. Kim, J. A. Lim, D. Kwak, S. Lee and K. Cho, *Adv. Mater.*, 2009, **21**, 1349.
11 W. H. Lee, J. A. Lim, D. Kwak, J. H. Cho, H. S. Lee, H. H. Choi and K. Cho, *Adv. Mater.*, 2009, **21**, 4243.
12 Y. D. Park, J. A. Lim, H. S. Lee and K. Cho, *Mater. Today*, 2007, **10**, 46.
13 C. A. Di, Y. Q. Liu, G. Yu and D. B. Zhu, *Acc. Chem. Res.*, 2009, **42**, 1573.
14 M. H. Yoon, C. Kim, A. Facchetti and T. J. Marks, *J. Am. Chem. Soc.*, 2006, **128**, 12851.
15 D. B. A. Rep, A. F. Morpurgo, W. G. Sloof and T. M. Klapwijk, *J. Appl. Phys.*, 2003, **93**, 2082.
16 S. J. Zilker, C. Detcheverry, E. Cantatore and D. M. de Leeuw, *Appl. Phys. Lett.*, 2001, **79**, 1124.
17 C. Goldmann, D. J. Gundlach and B. Batlogg, *Appl. Phys. Lett.*, 2006, **88**, 063501.
18 S. R. Forrest, *Chem. Rev.*, 1997, **97**, 1793.
19 R. Ruiz, D. Choudhary, B. Nickel, T. Toccoli, K. C. Chang, A. C. Mayer, P. Clancy, J. M. Blakely, R. L. Headrick, S. Iannotta and G. G. Malliaras, *Chem. Mater.*, 2004, **16**, 4497.
20 S. Verlaak, S. Steudel, P. Heremans, D. Janssen and M. S. Deleuze, *Phys. Rev. B: Condens. Matter Mater. Phys.*, 2003, **68**, 195409.
21 F. J. M. Z. Heringdorf, M. C. Reuter and R. M. Tromp, *Nature*, 2001, **412**, 517.
22 T. Yamaguchi, *J. Phys. Soc. Jpn.*, 1999, **68**, 1321.
23 C. B. France, P. G. Schroeder, J. C. Forsythe and B. A. Parkinson, *Langmuir*, 2003, **19**, 1274.
24 M. Shtein, J. Mapel, J. B. Benziger and S. R. Forrest, *Appl. Phys. Lett.*, 2002, **81**, 268.
25 K. Shankar and T. N. Jackson, *J. Mater. Res.*, 2004, **19**, 2003.
26 A. Ulman, *Chem. Rev.*, 1996, **96**, 1533.
27 S. Onclin, B. J. Ravoo and D. N. Reinhoudt, *Angew. Chem., Int. Ed.*, 2005, **44**, 6282.
28 S. A. DiBenedetto, A. Facchetti, M. A. Ratner and T. J. Marks, *Adv. Mater.*, 2009, **21**, 1407.
29 W. Gao, L. Dickinson, C. Grozinger, F. G. Morin and L. Reven, *Langmuir*, 1996, **12**, 6429.
30 C. R. Kagan, T. L. Breen and L. L. Kosbar, *Appl. Phys. Lett.*, 2001, **79**, 3536.
31 T. W. Kelley, L. D. Boardman, T. D. Dunbar, D. V. Muyres, M. J. Pellerite and T. Y. P. Smith, *J. Phys. Chem. B*, 2003, **107**, 5877.
32 H. Ma, O. Acton, G. Ting, J. W. Ka, H. L. Yip, N. Tucker, R. Schofield and A. K. Y. Jen, *Appl. Phys. Lett.*, 2008, **92**, 113303.
33 M. McDowell, I. G. Hill, J. E. McDermott, S. L. Bernasek and J. Schwartz, *Appl. Phys. Lett.*, 2006, **88**, 073505.
34 I. G. Hill, C. M. Weinert, L. Kreplak and B. P. van Zyl, *Appl. Phys. A: Mater. Sci. Process.*, 2009, **95**, 81.
35 W. Kalb, P. Lang, M. Mottaghi, H. Aubin, G. Horowitz and M. Wuttig, *Synth. Met.*, 2004, **146**, 279.
36 M. Mottaghi and G. Horowitz, *Org. Electron.*, 2006, **7**, 528.
37 Y. Y. Lin, D. J. Gundlach, S. F. Nelson and T. N. Jackson, *IEEE Electron Device Lett.*, 1997, **18**, 606.
38 S. Kobayashi, T. Nishikawa, T. Takenobu, S. Mori, T. Shimoda, T. Mitani, H. Shimotani, N. Yoshimoto, S. Ogawa and Y. Iwasa, *Nat. Mater.*, 2004, **3**, 317.
39 H. Yang, T. J. Shin, M. M. Ling, K. Cho, C. Y. Ryu and Z. N. Bao, *J. Am. Chem. Soc.*, 2005, **127**, 11542.
40 G. C. Yuan, Z. S. Lu, Z. Xu, C. Gong, Q. L. Song, S. L. Zhao, F. J. Zhang, N. Xu, Y. Gan, H. B. Yang and C. M. Li, *Org. Electron.*, 2009, **10**, 1388.
41 S. M. Jeong and J. W. Park, *J. Am. Chem. Soc.*, 2008, **130**, 3497.
42 P. Dhagat, H. M. Haverinen, R. J. Kline, Y. Jung, D. A. Fischer, D. M. DeLongchamp and G. E. Jabbour, *Adv. Funct. Mater.*, 2009, **19**, 2365.
43 D. Kumaki, S. Ando, S. Shimono, Y. Yamashita, T. Umeda and S. Tokito, *Appl. Phys. Lett.*, 2007, **90**, 053506.
44 D. H. Kim, H. S. Lee, H. Yang, L. Yang and K. Cho, *Adv. Funct. Mater.*, 2008, **18**, 1363.
45 H. S. Lee, D. H. Kim, J. H. Cho, M. Hwang, Y. Jang and K. Cho, *J. Am. Chem. Soc.*, 2008, **130**, 10556.
46 A. Virkar, S. Mannsfeld, J. H. Oh, M. F. Toney, Y. H. Tan, G. Y. Liu, J. C. Scott, R. Miller and Z. Bao, *Adv. Funct. Mater.*, 2009, **19**, 1962.
47 H. S. Lee, H. H. Choi, Y. D. Park, W. H. Lee and K. Cho, unpublished results.
48 Y. B. Jin, Z. L. Rang, M. I. Nathan, P. P. Ruden, C. R. Newman and C. D. Frisbie, *Appl. Phys. Lett.*, 2004, **85**, 4406.
49 H. Yang, S. H. Kim, L. Yang, S. Y. Yang and C. E. Park, *Adv. Mater.*, 2007, **19**, 2868.
50 W. Y. Chou, C. W. Kuo, H. L. Cheng, Y. R. Chen, F. C. Tang, F. Y. Yang, D. Y. Shu and C. C. Liao, *Appl. Phys. Lett.*, 2006, **89**, 112126.
51 Y. X. Lu, W. H. Lee, H. S. Lee, Y. Jang and K. Cho, *Appl. Phys. Lett.*, 2009, **94**, 113303.
52 C. Kim, A. Facchetti and T. J. Marks, *Science*, 2007, **318**, 76.
53 X. L. Duan, Q. X. Tang, J. Qiu, Y. H. Niu, Z. G. Wang and W. P. Hu, *Appl. Phys. Lett.*, 2009, **95**, 113301.
54 W. Y. Chou and H. L. Cheng, *Adv. Funct. Mater.*, 2004, **14**, 811.
55 M. L. Swiggers, G. Xia, J. D. Slinker, A. A. Gorodetsky, G. G. Malliaras, R. L. Headrick, B. T. Weslowski, R. N. Shashidhar and C. S. Dulcey, *Appl. Phys. Lett.*, 2001, **79**, 1300.
56 S. Z. Weng, W. S. Hu, C. H. Kuo, Y. T. Tao, L. J. Fan and Y. W. Yang, *Appl. Phys. Lett.*, 2006, **89**, 172103.
57 S. J. Kang, Y. Y. Noh, K. J. Baeg, J. Ghim, J. H. Park, D. Y. Kim, J. S. Kim, J. H. Park and K. Cho, *Appl. Phys. Lett.*, 2008, **92**, 052107.
58 H. Sirringhaus, *Adv. Mater.*, 2005, **17**, 2411.
59 A. Salleo, *Mater. Today*, 2007, **10**, 38.
60 L. L. Chua, P. K. H. Ho, H. Sirringhaus and R. H. Friend, *Appl. Phys. Lett.*, 2004, **84**, 3400.
61 J. Veres, S. D. Ogier, S. W. Leeming, D. C. Cupertino and S. M. Khaffaf, *Adv. Funct. Mater.*, 2003, **13**, 199.
62 J. Y. Liu, R. Zhang, G. Sauve, T. Kowalewski and R. D. McCullough, *J. Am. Chem. Soc.*, 2008, **130**, 13167.
63 H. Yan, Z. H. Chen, Y. Zheng, C. Newman, J. R. Quinn, F. Dotz, M. Kastler and A. Facchetti, *Nature*, 2009, **457**, 679–U671.

64 H. Sirringhaus, P. J. Brown, R. H. Friend, M. M. Nielsen, K. Bechgaard, B. M. W. Langeveld-Voss, A. J. H. Spiering, R. A. J. Janssen, E. W. Meijer, P. Herwig and D. M. de Leeuw, *Nature*, 1999, **401**, 685.
65 H. Sirringhaus, N. Tessler and R. H. Friend, *Science*, 1998, **280**, 1741.
66 J. F. Chang, B. Q. Sun, D. W. Breiby, M. M. Nielsen, T. I. Solling, M. Giles, I. McCulloch and H. Sirringhaus, *Chem. Mater.*, 2004, **16**, 4772.
67 J. Veres, S. Ogier, G. Lloyd and D. de Leeuw, *Chem. Mater.*, 2004, **16**, 4543.
68 S. Grecu, A. Roggenbuck, A. Opitz and W. Brutting, *Org. Electron.*, 2006, **7**, 276.
69 R. J. Kline, M. D. McGehee, E. N. Kadnikova, J. S. Liu, J. M. J. Frechet and M. F. Toney, *Macromolecules*, 2005, **38**, 3312.
70 R. J. Kline, M. D. McGehee and M. F. Toney, *Nat. Mater.*, 2006, **5**, 222.
71 D. H. Kim, Y. D. Park, Y. S. Jang, H. Yang, Y. H. Kim, J. I. Han, D. G. Moon, S. J. Park, T. Y. Chang, C. W. Chang, M. K. Joo, C. Y. Ryu and K. Cho, *Adv. Funct. Mater.*, 2005, **15**, 77.
72 D. H. Kim, Y. Jang, Y. D. Park and K. Cho, *Langmuir*, 2005, **21**, 3203.
73 D. H. Kim, Y. Jang, Y. D. Park and K. Cho, *Macromolecules*, 2006, **39**, 5843.
74 R. J. Kline, D. M. DeLongchamp, D. A. Fischer, E. K. Lin, L. J. Richter, M. L. Chabinyc, M. F. Toney, M. Heeney and I. McCulloch, *Macromolecules*, 2007, **40**, 7960.
75 K. Kaneto, W. Y. Lim, W. Takashima, T. Endo and M. Rikukawa, *Jpn. J. Appl. Phys.*, 2000, **39**, L872.
76 Y. D. Park, D. H. Kim, Y. Jang, J. H. Cho, M. Hwang, H. S. Lee, J. A. Lim and K. Cho, *Org. Electron.*, 2006, **7**, 514.
77 B. S. Ong, Y. L. Wu, P. Liu and S. Gardner, *J. Am. Chem. Soc.*, 2004, **126**, 3378.
78 B. S. Ong, Y. L. Wu, P. Liu and S. Gardner, *Adv. Mater.*, 2005, **17**, 1141.
79 Y. O. Wu, P. Liu, B. S. Ong, T. Srikumar, N. Zhao, G. Botton and S. P. Zhu, *Appl. Phys. Lett.*, 2005, **86**, 142102.
80 Y. L. Wu, P. Liu and B. S. Ong, *Appl. Phys. Lett.*, 2006, **89**, 013505.
81 I. Mcculloch, M. Heeney, C. Bailey, K. Genevicius, I. Macdonald, M. Shkunov, D. Sparrowe, S. Tierney, R. Wagner, W. M. Zhang, M. L. Chabinyc, R. J. Kline, M. D. Mcgehee and M. F. Toney, *Nat. Mater.*, 2006, **5**, 328.
82 M. L. Chabinyc, M. F. Toney, R. J. Kline, I. McCulloch and M. Heeney, *J. Am. Chem. Soc.*, 2007, **129**, 3226.
83 R. J. Kline, D. M. DeLongchamp, D. A. Fischer, E. K. Lin, M. Heeney, I. McCulloch and M. F. Toney, *Appl. Phys. Lett.*, 2007, **90**, 062117.
84 T. Umeda, S. Tokito and D. Kumaki, *J. Appl. Phys.*, 2007, **101**, 054517.
85 T. Umeda, D. Kumaki and S. Tokito, *J. Appl. Phys.*, 2009, **105**, 024516.
86 R. J. Kline, M. D. McGehee, E. N. Kadnikova, J. S. Liu and J. M. J. Frechet, *Adv. Mater.*, 2003, **15**, 1519.
87 A. Zen, J. Pflaum, S. Hirschmann, W. Zhuang, F. Jaiser, U. Asawapirom, J. P. Rabe, U. Scherf and D. Neher, *Adv. Funct. Mater.*, 2004, **14**, 757.
88 J. S. Liu, E. Sheina, T. Kowalewski and R. D. McCullough, *Angew. Chem., Int. Ed.*, 2002, **41**, 329.
89 X. L. Chen, A. J. Lovinger, Z. N. Bao and J. Sapjeta, *Chem. Mater.*, 2001, **13**, 1341.
90 H. Heil, T. Finnberg, N. von Malm, R. Schmechel and H. von Seggern, *J. Appl. Phys.*, 2003, **93**, 1636.
91 K. R. Amundson, B. J. Sapjeta, A. J. Lovinger and Z. N. Bao, *Thin Solid Films*, 2002, **414**, 143.
92 T. Fujiwara, J. Locklin and Z. N. Bao, *Appl. Phys. Lett.*, 2007, **90**, 232108.
93 G. F. Xu, Z. A. Bao and J. T. Groves, *Langmuir*, 2000, **16**, 1834.
94 M. M. Ling and Z. N. Bao, *Chem. Mater.*, 2004, **16**, 4824.
95 S. H. Liu, W. C. M. Wang, A. L. Briseno, S. C. E. Mannsfeld and Z. N. Bao, *Adv. Mater.*, 2009, **21**, 1217.
96 S. Nagamatsu, W. Takashima, K. Kaneto, Y. Yoshida, N. Tanigaki and K. Yase, *Macromolecules*, 2003, **36**, 5252.
97 S. Nagamatsu, W. Takashima, K. Kaneto, Y. Yoshida, N. Tanigaki and K. Yase, *Appl. Phys. Lett.*, 2004, **84**, 4608.
98 G. Derue, S. Coppee, S. Gabriele, M. Surin, V. Geskin, F. Monteverde, P. Leclere, R. Lazzaroni and P. Damman, *J. Am. Chem. Soc.*, 2005, **127**, 8018.
99 H. Sirringhaus, R. J. Wilson, R. H. Friend, M. Inbasekaran, W. Wu, E. P. Woo, M. Grell and D. D. C. Bradley, *Appl. Phys. Lett.*, 2000, **77**, 406.
100 M. Brinkmann and P. Rannou, *Adv. Funct. Mater.*, 2007, **17**, 101.
101 M. Brinkmann and J. C. Wittmann, *Adv. Mater.*, 2006, **18**, 860.
102 L. H. Jimison, M. F. Toney, I. McCulloch, M. Heeney and A. Salleo, *Adv. Mater.*, 2009, **21**, 1568.
103 H. N. Tsao, D. Cho, J. W. Andreasen, A. Rouhanipour, D. W. Breiby, W. Pisula and K. Mullen, *Adv. Mater.*, 2009, **21**, 209.
104 D. M. DeLongchamp, R. J. Kline, Y. Jung, D. S. Germack, E. K. Lin, A. J. Moad, L. J. Richter, M. F. Toney, M. Heeney and I. McCulloch, *ACS Nano*, 2009, **3**, 780–787.
105 J. E. Anthony, *Chem. Rev.*, 2006, **106**, 5028.
106 M. Mas-Torrent and C. Rovira, *Chem. Soc. Rev.*, 2008, **37**, 827.
107 J. A. Lim, H. S. Lee, W. H. Lee and K. Cho, *Adv. Funct. Mater.*, 2009, **19**, 1515.
108 W. Pisula, A. Menon, M. Stepputat, I. Lieberwirth, U. Kolb, A. Tracz, H. Sirringhaus, T. Pakula and K. Mullen, *Adv. Mater.*, 2005, **17**, 684.
109 C. M. Duffy, J. W. Andreasen, D. W. Breiby, M. M. Nielsen, M. Ando, T. Minakata and H. Sirringhaus, *Chem. Mater.*, 2008, **20**, 7252.
110 M. Cavallini, P. Stoliar, J. F. Moulin, M. Surin, P. Leclere, R. Lazzaroni, D. W. Breiby, J. W. Andreasen, M. M. Nielsen, P. Sonar, A. C. Grimsdale, K. Mullen and F. Biscarini, *Nano Lett.*, 2005, **5**, 2422.
111 M. Cavallini, C. Albonetti and F. Biscarini, *Adv. Mater.*, 2009, **21**, 1043.
112 W. H. Lee, D. H. Kim, Y. Jang, J. H. Cho, M. Hwang, Y. D. Park, Y. H. Kim, J. I. Han and K. Cho, *Appl. Phys. Lett.*, 2007, **90**, 132106.
113 J. Rivnay, L. H. Jimison, J. E. Northrup, M. F. Toney, R. Noriega, S. F. Lu, T. J. Marks, A. Facchetti and A. Salleo, *Nat. Mater.*, 2009, **8**, 952.
114 J. A. Lim, W. H. Lee, H. S. Lee, J. H. Lee, Y. D. Park and K. Cho, *Adv. Funct. Mater.*, 2008, **18**, 229.
115 J. A. Lim, W. H. Lee, D. Kwak and K. Cho, *Langmuir*, 2009, **25**, 5404.
116 Z. M. Wei, Y. Cao, W. Z. Ma, C. L. Wang, W. Xu, X. F. Guo, W. P. Hu and D. B. Zhu, *Appl. Phys. Lett.*, 2009, **95**, 033304.
117 G. S. Tulevski, Q. Miao, M. Fukuto, R. Abram, B. Ocko, R. Pindak, M. L. Steigerwald, C. R. Kagan and C. Nuckolls, *J. Am. Chem. Soc.*, 2004, **126**, 15048.
118 X. F. Guo, M. Myers, S. X. Xiao, M. Lefenfeld, R. Steiner, G. S. Tulevski, J. Y. Tang, J. Baumert, F. Leibfarth, J. T. Yardley, M. L. Steigerwald, P. Kim and C. Nuckolls, *Proc. Natl. Acad. Sci. U. S. A.*, 2006, **103**, 11452.
119 M. Mottaghi, P. Lang, F. Rodriguez, A. Rumyantseva, A. Yassar, G. Horowitz, S. Lenfant, D. Tondelier and D. Vuillaume, *Adv. Funct. Mater.*, 2007, **17**, 597.
120 E. C. P. Smits, S. G. J. Mathijssen, P. A. van Hal, S. Setayesh, T. C. T. Geuns, K. A. H. A. Mutsaers, E. Cantatore, H. J. Wondergem, O. Werzer, R. Resel, M. Kemerink, S. Kirchmeyer, A. M. Muzafarov, S. A. Ponomarenko, B. de Boer, P. W. M. Blom and D. M. de Leeuw, *Nature*, 2008, **455**, 956.
121 S. G. J. Mathijssen, E. C. P. Smits, P. A. van Hal, H. J. Wondergem, S. A. Ponomarenko, A. Moser, R. Resel, P. A. Bobbert, M. Kemerink, R. A. J. Janssen and D. M. de Leeuw, *Nat. Nanotechnol.*, 2009, **4**, 674.
122 J. Collet, O. Tharaud, A. Chapoton and D. Vuillaume, *Appl. Phys. Lett.*, 2000, **76**, 1941.
123 M. Halik, H. Klauk, U. Zschieschang, G. Schmid, C. Dehm, M. Schutz, S. Maisch, F. Effenberger, M. Brunnbauer and F. Stellacci, *Nature*, 2004, **431**, 963.
124 H. Klauk, U. Zschieschang, J. Pflaum and M. Halik, *Nature*, 2007, **445**, 745.
125 Y. D. Park, D. H. Kim, Y. Jang, M. Hwang, J. A. Lim and K. Cho, *Appl. Phys. Lett.*, 2005, **87**, 243509.
126 H. Sirringhaus, *Adv. Mater.*, 2009, **21**, 3859.